To Understand Film Dynamics Look to the Bulk

Ronald P. White and Jane E. G. Lipson*
Department of Chemistry, Dartmouth College, Hanover, New Hampshire 03755, USA

(Received 12 May 2020; revised 27 June 2020; accepted 8 July 2020; published 30 July 2020)

We show that shifts in dynamics of confined systems relative to that of the bulk material originate in the properties of bulk alone, and exhibit the same form of behavior as when different bulk isobars are compared. For bulk material, pressure-dependent structural relaxation times follow $\tau(T,V) \propto \exp[f(T) \times g(V)]$. When two states (isobars) of the material, "1" and "2", are compared at the same temperature this leads to a form $\tau_2 \propto \tau_1^c$, where $c = g[V_2(T)]/g[V_1(T)]$. Using equation of state analysis and two models for P-dependent dynamics, we show that c is approximately T independent, and that it can be very simply expressed in terms of either the (free) volume above the close packed state (V_{free}) or the activation energy for cooperative motion. The effect of changing state through a shift in pressure (P_1 to P_2) is thus mechanistically traceable to cooperativity changing with density, through V_{free}. The connection with confined dynamics follows when 1 and 2 are taken as bulk and film at ambient P, differing in density only due to the film surface. The general form for $\tau(T,V)$ also illuminates why samples in different states (film vs bulk, high P vs low) trend toward the same relaxation behavior at high T.

DOI: 10.1103/PhysRevLett.125.058002

Over the last three decades there has been significant research interest aimed at understanding how a system's structural dynamics is affected by the presence of an interface [1–14]. This "nanoconfinement effect" is seen in polymer thin films, whose behavior is affected by the presence of free surfaces and/or various types of substrate interfaces. Experiment and simulation have shown film segmental relaxation times may differ from bulk depending on film thickness, film preparation, temperature, and the types of interfaces involved. Here, we focus on the segmental (α) relaxation of glass forming materials, e.g., as measured via dielectric spectroscopy [1,9,12,13]. Recently, we among others have noted [15–21] an apparent analogy between pressure (density) changes and the effects observed in nanoconfined systems. In this Letter we show that understanding what controls a material's *bulk* pressure-dependent dynamics [22,23] provides essential insight into the confinement effect on dynamic response.

Experiment has shown bulk relaxation times follow a general form

$$\tau(T,V) \propto \exp[f(T) \times g(V)] \tag{1}$$

with a T-based contribution $f(T)$, and V-based contribution $g(V)$; two models that describe these functions will be introduced further below. A key theme here is that $f(T)$ and $g(V)$ are *multiplicatively* coupled in the exponential.

The framework of Eq. (1) accounts independently for variations in density and temperature. In confined systems we expect density differences to play an important role. However, density in these systems (e.g., polymer films) is challenging to measure experimentally [24–26]. In the case of a free surface, it is clear that the local density profile $\rho(z)$ changes from bulk density to zero, and so a fraction of segments must experience an environment of lowered density. However, the relaxation profile $\tau(z)$ will not track directly with $\rho(z)$. Simulation results [5,27–29] show that the gradient in $\tau(z)$ is wider than that of $\rho(z)$. For example, $\rho(z)$ could be at the bulk density at a given position z from the free surface, while the *average* over a single near neighbor distance could yield a value closer to half of that. Indeed the gradient in $\rho(z)$ can be very narrow, $\approx$1 nm wide [30], while a molecular (Kuhn) segment is $\approx$1.5 nm [31]. As density in the bulk effectively characterizes *intermolecular* crowding, the relevant density in inhomogeneous environments must therefore be an average of $\rho(z)$ over a sensible intermolecular scale, e.g., 2, 3 Kuhn segments. In fact, this $\sim$5 nm length scale is similar to measurements of mobile layer thickness [32]. Lower densities may also occur near a supporting substrate interface [11,19,21,33,34]. Probe adsorption measurements [33,34] demonstrated added free space from inefficient packing of polymer chains following spin coating, and AFM measurements [21] have shown open pockets of free space near asperities on rough substrates. Additional details may be found in the Supplemental Material [35] and the appendix of Ref. [18].

When compared at the same temperature, the relaxation time of a confined, relative to a corresponding bulk, sample can be expressed as $\tau_{\text{film}} \propto \tau_{\text{bulk}}^c$, where the power law exponent (c) has been ascribed [6,36] to the nanoconfinement effect. In Diaz-Vela *et al.* [36], c was called the "decoupling exponent," a constant multiplicative factor that scales the bulk activation energy (sufficient at any given T).

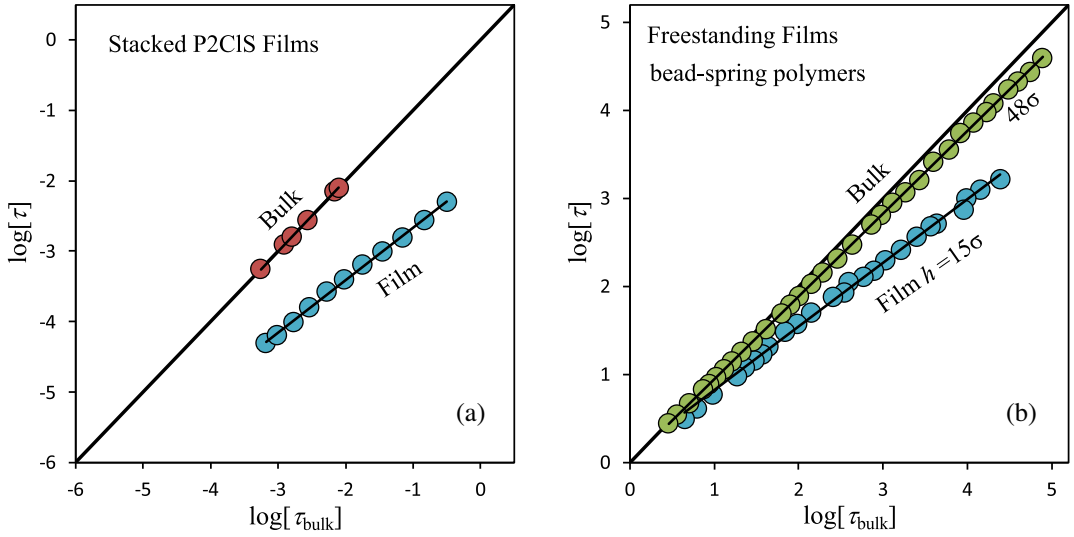

FIG. 1. Film relaxation times plotted vs bulk relaxation times at the same T. (a) α relaxation times [37] for 18 nm stacked P2ClS films (before annealing) vs bulklike relaxation times for 120 nm films. (b) Molecular dynamics simulation results [36], film thicknesses of 15σ and 47σ.

In a confined system c depends on film thickness h or, in other more resolved experiments, it can be ascribed to a position in the film z.

Experimental results that demonstrate confinement effects are shown in Fig. 1(a) for the case of stacked poly 2-chlorostyrene films (taken from Fukao *et al.* [37]); in Fig. 1(b), simulation results (taken from Diaz-Vela *et al.* [36]) are shown for freestanding films of bead-spring polymers. The plots show $\log \tau_{\text{film}}$ plotted against $\log \tau_{\text{bulk}}$ for sets of film data at a fixed thickness. In both plots the bulk behavior falls on the diagonal; in the case of the Fukao *et al.* [37] data results (red symbols) were collected on a film 120 nm thick, and interpreted as representing bulk behavior. Each of the other points represents a comparison between τ_{film} and τ_{bulk} at the same T; traveling upward along the line from left to right, T is decreasing. The results for each film thickness fall on lines having slope c, the power law exponent. The results from both plots illustrate that deviation from bulk increases as T decreases (left to right). The simulation results (b) also show that thinner films deviate more strongly than thicker ones from bulk behavior.

In Fig. 2 we turn to the bulk, and show that the same form of behavior (Fig. 1) is manifest in bulk samples, alone, when comparing results at different temperatures and densities. We plot experimental relaxation times [38,39] for bulk polyvinyl acetate (PVAC) on two isobars ($P = 1$ atm and 100 MPa). The 100 MPa isobar is treated as the "reference" here because it is at higher density, making the lower density 1 atm isobar analogous to the situation for the lower density freestanding, or stacked freestanding, films. The relaxation times of the 1 atm isobar are plotted against those of the 100 MPa isobar, with each point taken at the same temperature. As was the case for the films, the lower density (1 atm bulk isobar) sample shows a characteristic average slope that is different (smaller) compared to the higher density (100 MPa bulk isobar, i.e., the diagonal line) sample.

The results in Fig. 2 will follow a power law behavior analogous to that shown by data for confined systems, and we can now show why this is expected. We denote the two isobars as "1" (100 MPa) and "2" (1 atm), and the temperature-dependent volume on each isobar as $V_1(T)$ and $V_2(T)$. Using Eq. (1), the relaxation time, $\tau_2(T) \propto \exp\{f(T) \times g[V_2(T)]\}$, is then written in terms of the value

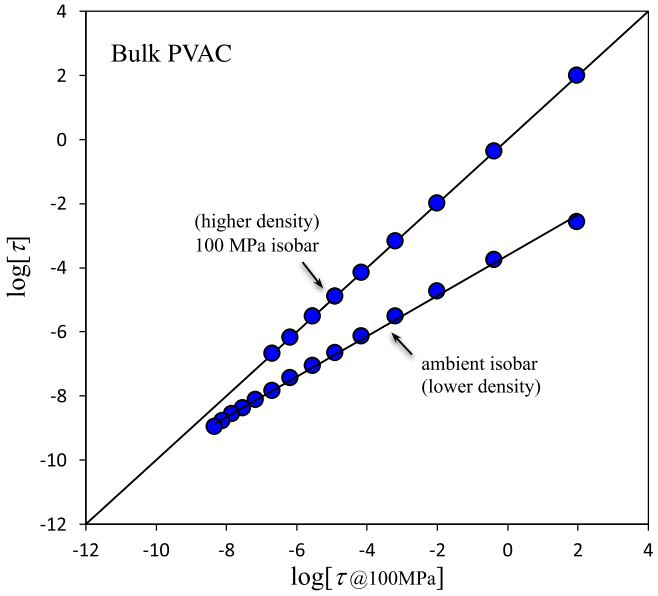

FIG. 2. PVAC α relaxation times [38]; the log of relaxation times for the 1 atm isobar are plotted against those of the (denser) 100 MPa isobar at the same temperature.

of $\tau_1(T) \propto \exp\{f(T) \times g[V_1(T)]\}$ at the same T. This leads to

$$\tau_2(T) \propto \{\exp\{f(T) \times g[V_1(T)]\}\}^{g[V_2(T)]/g[V_1(T)]}, \quad (2)$$

and thus equivalently $\tau_2(T) \propto \tau_1(T)^c$, where we identify

$$c = g[V_2(T)]/g[V_1(T)]. \quad (3)$$

As the $\ln \tau_2$ vs $\ln \tau_1$ plots (Figs. 1 and 2) are approximately linear, this indicates that $c = g[V_2(T)]/g[V_1(T)]$ must remain approximately constant even though both $V_1(T)$ and $V_2(T)$ change with T. Indeed, we can verify this using two different models for pressure-dependent dynamics.

One is the density scaling model [40–44]

$$\tau = \tau_0 \exp\left[\frac{A^\phi}{T^\phi V^{\gamma\phi}}\right], \quad (4)$$

where γ, ϕ, A, and τ_0 are four material specific parameters, and where $f(T) \propto 1/T^\phi$ and $g(V) \propto 1/V^{\gamma\phi}$. We also apply the cooperative free volume (CFV) rate model [18,45,46]

$$\tau = \tau_{\text{ref}} \exp\left[\frac{T^{*b}}{T^b}\frac{V_{\text{hc}}}{V_{\text{free}}}\right], \quad (5)$$

where b, T^*, and τ_{ref}, are material specific parameters, and where $f(T) \propto 1/T^b$ and $g(V) \propto 1/V_{\text{free}}$. $V_{\text{free}} = V - V_{\text{hc}}$ is defined [47] as the difference between a system's overall volume V and its limiting, closely packed, hard core value, V_{hc}. V_{hc} is a constant, independent of the dynamics, from analysis of thermodynamic (PVT) data using the locally correlated lattice model (LCL) equation of state (EOS). [47] Both models have been applied to express the pressure-dependent dynamics of PVAC. Background on the models is available in the Supplemental Material [35].

The CFV model yields $c = g[V_2(T)]/g[V_1(T)] = V_{\text{free:1}}(T)/V_{\text{free:2}}(T)$. Figure 3 illustrates that this ratio indeed remains approximately constant as temperature is varied. Here, results based on the LCL EOS analysis of PVAC PVT data [48] are shown for $V_{\text{free:1}}(T)$ at $P =$ 100 MPa, and $V_{\text{free:2}}(T)$ at $P = 1$ atm. Multiplication of the $V_{\text{free:2}}(T)$ curve by a *single constant* produces a curve that overlaps very well with the $V_{\text{free:1}}(T)$ curve, and from this we thus estimate a value of $c \approx 0.66$ (the value that gives the best overlap). In the case of the density scaling model, we have plotted $V_1^{\gamma\phi}(T)$ and $V_2^{\gamma\phi}(T)$ in the inset of Fig. 3. Here, we have taken the $\gamma = 2.34$ and $\phi = 4.71$ values from Casalini and Roland [41]; the values for V are in mL/g and come from fitting the Tait equation [49] to the PVT data. These results show that the curves overlap using a constant multiplicative shift, verifying that $g[V_2(T)]/g[V_1(T)] = V_1^{\gamma\phi}(T)/V_2^{\gamma\phi}(T)$ has an approximately constant value of $c \approx 0.61$. Note that both of these model-based

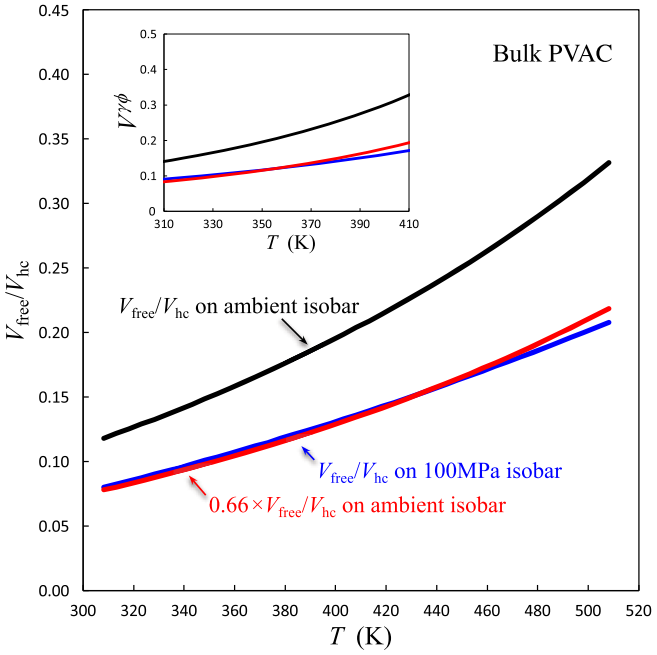

FIG. 3. PVAC volume-based contribution to dynamics $g(V)$ for $P = 1$ atm (black) and 100 MPa (blue) isobars based on EOS analysis of PVT data [48]. The red curve corresponds to the 1 atm isobar multiplied by a constant shift factor. Main plot (CFV rate model): $1/g(V) = V_{\text{free}}/V_{\text{hc}}$ vs T. Inset (density scaling model): $1/g(V) = V^{\gamma\phi}$ vs T.

estimates for c are in very close agreement with the raw trends in Fig. 2, which follow directly from the experimental relaxation times; in this case the slope of the $\ln \tau_2$ vs $\ln \tau_1$ power law plot is approximately $c \approx 0.63$.

Both the CFV and density scaling models demonstrate that the physical significance of $c < 1$ is that the density of 2 is lowered (for CFV this corresponds to higher V_{free}) compared to the reference system 1, and thus the dynamics are faster, $\tau_2 = \tau_1^c < \tau_1$. This reasoning applies broadly; it explains trends in the two bulk isobars, as well as in the results for film vs bulk.

From this point onward we apply the 1 and 2 notation in the general sense: These can be either two bulk isobars, or, bulk and film isobars, say at ambient pressure (1 atm), with $V_1(T)$ and $V_2(T)$ differing due to the presence of film interfaces. The density that describes a film, which has a nonhomogeneous local density, would be the value averaged over the cooperative length scale. [18] In all cases we expect $V_1(T)$ and $V_2(T)$ will increase with T, and the $c = g[V_2(T)]/g[V_1(T)]$ ratio will be approximately constant, as illustrated in Fig. 3 for PVAC. [Another case would be two isochors, where $c = g(V_2)/g(V_1)$ must be constant.]

We now return to the fundamental $\tau(T, V) \propto \exp[f(T) \times g(V)]$ relationship to emphasize some important points. The key to deriving the $\tau_2 \propto \tau_1^c$ result for two bulk isobars above relied on the fact that the same function $f(T)$ applies for both isobars, 1 and 2. [Indeed, $f(T)$ must apply at any

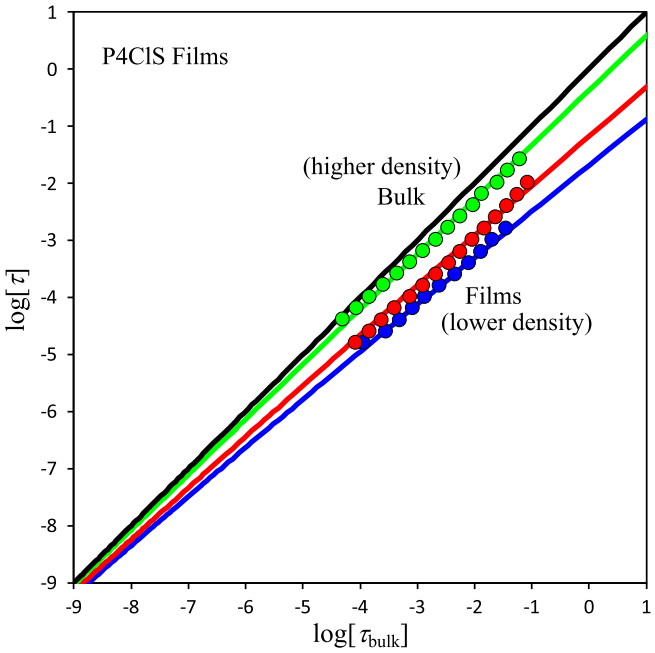

FIG. 4. Relaxation times for Al-capped P4ClS films: $\log\tau$ vs $\log\tau_{\rm bulk}$ at the same temperature. Experimental data (symbols), CFV model (curves) for bulk (black), and 71 nm (green), 21 nm (red), and 14 nm (blue) films.

density in a bulk pressure-dependent dynamics description.] However, given that the bulk isobar-film isobar scenario has been shown to exhibit the same $\tau_2 \propto \tau_1^c$ form of behavior, we can conclude the following: The same function $f(T)$ that works for the bulk material must also be sufficient (at least approximately) for describing the T-dependent contribution to the dynamics in films.

In fact, we have already made this very assumption in our CFV model for polymer films [18], which has been tested experimentally [19]. More examples of successfully using the bulk functional form $f(T)$ for (isobaric) polymers and (isochoric) small molecules in confinement can be found in Adrjanowicz *et al.* [16,20] where the authors applied the density scaling model.

We now apply the above analysis to nanoconfined systems using our CFV film results, along with experimental data; both are shown in Fig. 4 (from Ref. [19]) for poly(4-chlorostyrene) (P4ClS) films. (See Supplemental Material [35] for details on the CFV film model.) Here, the plots are in the $\ln\tau_2$ vs $\ln\tau_1$ representation, and they confirm the same power law form as the results in Figs. 1 and 2. The Fig. 4 plot also clearly shows that the linear slope (power law exponent, c) decreases with film thickness (h). Now we are in a position to explain this trend.

Our new analysis shows that the volume-based contribution to the shift in *film* dynamics follows model prediction for the effect of a density shift in *bulk* dynamics. In both cases this plays out through the free volume ratio $V_{\rm free:1}(T)/V_{\rm free:2}(T)$. A thinner film sample (2)–analogous to a bulk sample at lower pressure—has a larger relative $V_{\rm free}$. In the nanoconfined experiment this is due to the larger "voice" of the lower density interfacial region in a very thin film. The result is that the free volume ratio—which translates as the slope of the plot—decreases with film thickness (or bulk sample pressure).

We can compare the power law slopes c for films of comparable thickness in Figs. 1, 2, and 4 where, in each case, we average over all the data in determining the slope. The freestanding 15σ bead-spring films, 18 nm stacked P2ClS films, and 14 nm Al-capped P4ClS films have $c \approx 0.72$, 0.75, and 0.84 respectively. We see across results from different methods that comparable film thicknesses have comparable values of c. Within this group we note that the stacked P2ClS films have greater free surface area, hence a more reduced density relative to bulk, than the Al-capped P4ClS films, where the decrease comes from inefficient packing near the substrate interface. This is reflected in a lower c for the former than the latter. Turning to the *bulk* PVAC isobars, $c = 0.66$ was obtained in Fig. 3 in shifting from $P = 100$ MPa to 1 atm ($V_{\rm free}/V_{\rm hc}$ changing from 0.101 to 0.149 at $T = 350$ K). By the same analysis, shifts of 50 MPa to 1 atm, and 25 MPa to 1 atm, give $c = 0.79$ and 0.88, respectively. The effect of changing pressure on bulk samples yields c values that are very similar to those that reflect shifting from bulk to thin film. To give a sense for c in terms of density changes, the PVAC values of $c = 0.66$, 0.79, and 0.88 correspond (at $T = 350$ K) to density changes of 4.2%, 2.4%, and 1.3%, respectively. Consistent with these values, CFV calculations in Ref. [19] gave a density change of 2.0% for the 14 nm P4ClS film compared to bulk (433 K).

These results also allow us to relate changing film thickness, or bulk pressure effects, to shifts in activation energy ($E_{\rm act}$) and local cooperativity for segmental relaxation. Using Eq. (1) we can write $E_{\rm act}(T,V) = RTf(T)g(V)$, and on any particular isobar, $V(T)$,

$$E_{\rm act}(T) = RTf(T)g[V(T)]. \tag{6}$$

As noted above, Diaz-Vela *et al.* [36] described the exponent c as a constant multiplicative factor that scales the T-dependent bulk activation energy $E_{\rm act}(T)$ at any given T, into that of the film. This leads to $E_{\rm act:2}(T) = cE_{\rm act:1}(T)$, where $c = E_{\rm act:2}(T)/E_{\rm act:1}(T) \approx$ constant.

Once again, this simple result only works well as long as the same functional form $f(T)$ applies for both bulk and film. If that is true then it follows from Eq. (6) that $E_{\rm act:2}(T)/E_{\rm act:1}(T) = g[V_2(T)]/g[V_1(T)] = c \approx$ constant (the latter equalities were shown above). Note that this condition is supported by experiment. If the functional T dependence differed for bulk and film—say $f_1(T)$ for bulk and $f_2(T)$ for film—then, the ratio $f_2(T)/f_1(T)$ would survive to appear in c and would show up as a residual T dependence in the slope of the film plots.

We can go further by applying the CFV model. From Eq (5), $E_{\mathrm{act}}(T) = RTf(T)g[V(T)] \propto (1/T^{b-1})[1/V_{\mathrm{free}}(T)]$ for any given isobar. The CFV rate model is based on a mechanism [46] where a number (n^*) of segments must cooperate to open up enough total space to promote a relaxation event. n^* increases with density which changes the activation energy according to $E_{\mathrm{act}} \propto n^* \propto 1/V_{\mathrm{free}}$.

The CFV model relates the E_{act} required for thermal activation to the inverse free volume. This explains the origin of the result that P-dependent dynamics follows the fundamental $\tau(T,V) \propto \exp[f(T) \times g(V)]$ form, showing *multiplicative* dependence of relaxation times on T and V. (See the Supplemental Material [35].) For CFV the 2:1 activation energy ratio yields a very simple result: $E_{\mathrm{act:2}}(T)/E_{\mathrm{act:1}}(T) = V_{\mathrm{free:1}}(T)/V_{\mathrm{free:2}}(T) = c$.

Using the above, the CFV model also equates the power law exponent to the ratio of the number of cooperating segments $c = n_2^*/n_1^*$ required in the two states (film or bulk, lower pressure or higher). The model directly connects shifts in density with corresponding shifts in activation energy and degree of cooperativity. Since the entropy-based model of Adam and Gibbs [50], cooperativity has been important in explaining glassy dynamics; these CFV model results provide a novel route for interpretation.

As a final point, we explain the evident insensitivity of relaxation times to either confinement (Figs. 1 and 4) or pressure (Fig. 2) effects at high temperatures. For the ratio of the relaxation times associated with states 1 and 2 Eq. (1) gives

$$\tau_2(T)/\tau_1(T) \propto \exp\{f(T) \times (g[V_2(T)] - g[V_1(T)])\}. \quad (7)$$

Between film and bulk, or between a bulk sample at two very different pressures, we expect some nonzero difference in the volume-dependent contributions, $g[V_2(T)] - g[V_1(T)]$. However, the multiplicative form means that this difference is scaled by $f(T)$. Now, $f(T)$ increases as T is lowered, and it vanishes at high T. Thus, at high T there is little difference between τ_1 and τ_2 no matter how thin the film or how low the pressure. In addition, as is observed experimentally (e.g., Figs. 1, 2, and 4), the separation between 1 and 2 (the "sensitivity to confinement" in the case of films) will systematically grow as T decreases, and this is indeed the qualitative prediction of Eq. (7).

In conclusion, we have mapped a bright line connecting the impact of sample nanoconfinement on segmental dynamics to the effect of changing the thermodynamic state of a bulk sample. This analysis succeeds because the roles of temperature and density in altering dynamic response are multiplicatively linked. The simplicity of our model also leads to predictive power: characterization of bulk behavior alone allows us to anticipate how changing pressure and/or film thickness will affect sample free volume, local activation energies, and cooperativity requirements. The result is a deeper understanding of what drives segmental relaxation under a wide variety of sample conditions.

We gratefully acknowledge the financial support provided by the National Science Foundation (No. DMR-1708542).

*Corresponding author.
jane.lipson@dartmouth.edu

[1] S. Napolitano, E. Glynos, and N. B. Tito, Rep. Prog. Phys. **80**, 036602 (2017).
[2] M. D. Ediger and J. A. Forrest, Macromolecules **47**, 471 (2014).
[3] R. Richert, Annu. Rev. Phys. Chem. **62**, 65 (2011).
[4] M. Alcoutlabi and G. McKenna, J. Phys. Condens. Matter **17**, R461 (2005).
[5] D. S. Simmons, Macromol. Chem. Phys. **217**, 137 (2016).
[6] K. S. Schweizer and D. S. Simmons, J. Chem. Phys. **151**, 240901 (2019).
[7] J. Baschnagel and F. Varnik, J. Phys. Condens. Matter **17**, R851 (2005).
[8] D. Cangialosi, A. Alegria, and J. Colmenero, Prog. Polym. Sci. **54–55**, 128 (2016).
[9] V. M. Boucher, D. Cangialosi, H. Yin, A. Schoenhals, A. Alegria, and J. Colmenero, Soft Matter **8**, 5119 (2012).
[10] X. Monnier and D. Cangialosi, Phys. Rev. Lett. **121**, 137801 (2018).
[11] A. Panagopoulou and S. Napolitano, Phys. Rev. Lett. **119**, 097801 (2017).
[12] K. Fukao and Y. Miyamoto, Phys. Rev. E **61**, 1743 (2000).
[13] R. D. Priestley, D. Cangialosi, and S. Napolitano, J. Non-Cryst. Solids **407**, 288 (2015).
[14] F. Kremer, M. Tress, and E. U. Mapesa, J. Non-Cryst. Solids **407**, 277 (2015).
[15] K. Adrjanowicz, K. Kaminski, K. Koperwas, and M. Paluch, Phys. Rev. Lett. **115**, 265702 (2015).
[16] K. Adrjanowicz, K. Kaminski, M. Tarnacka, G. Szklarz, and M. Paluch, J. Phys. Chem. Lett. **8**, 696 (2017).
[17] M. Tarnacka, W. K. Kipnusu, E. Kaminska, S. Pawlus, K. Kaminski, and M. Paluch, Phys. Chem. Chem. Phys. **18**, 23709 (2016).
[18] R. P. White and J. E. G. Lipson, Macromolecules **51**, 7924 (2018).
[19] A. Debot, R. P. White, J. E. G. Lipson, and S. Napolitano, ACS Macro Lett. **8**, 41 (2019).
[20] K. Adrjanowicz, R. Winkler, A. Dzienia, M. Paluch, and S. Napolitano, ACS Macro Lett. **8**, 304 (2019).
[21] A. Panagopoulou, C. Rodríguez-Tinoco, R. P. White, J. E. G. Lipson, and S. Napolitano, Phys. Rev. Lett. **124**, 027802 (2020).
[22] C. Roland, S. Hensel-Bielowka, M. Paluch, and R. Casalini, Rep. Prog. Phys. **68**, 1405 (2005).
[23] G. Floudas, M. Paluch, A. Grzybowski, and K. Ngai, *Molecular Dynamics of Glass-Forming Systems: Effects of Pressure* (Springer, Berlin, 2011).
[24] X. Huang and C. B. Roth, J. Chem. Phys. **144**, 234903 (2016).

[25] A. B. Unni, G. Vignaud, J. P. Chapel, J. Giermanska, J. K. Bal, N. Delorme, T. Beuvier, S. Thomas, Y. Grohens, and A. Gibaud, Macromolecules **50**, 1027 (2017).
[26] S. Napolitano, Soft Matter **16**, 5348 (2020).
[27] P. Z. Hanakata, J. F. Douglas, and F. W. Starr, J. Chem. Phys. **137**, 244901 (2012).
[28] P. Z. Hanakata, B. A. P. Betancourt, J. F. Douglas, and F. W. Starr, J. Chem. Phys. **142**, 234907 (2015).
[29] D. M. Sussman, S. S. Schoenholz, E. D. Cubuk, and A. J. Liu, Proc. Natl. Acad. Sci. U. S. A. **114**, 10601 (2017).
[30] G. Dee and B. Sauer, Adv. Phys. **47**, 161 (1998).
[31] T. P. Lodge and T. C. B. McLeish, Macromolecules **33**, 5278 (2000).
[32] K. Paeng, S. F. Swallen, and M. D. Ediger, J. Am. Chem. Soc. **133**, 8444 (2011).
[33] S. Napolitano, S. Capponi, and B. Vanroy, Eur. Phys. J. E **36**, 61 (2013).
[34] S. Napolitano, C. Rotella, and M. Wubbenhorst, ACS Macro Lett. **1**, 1189 (2012).
[35] See Supplemental Material at http://link.aps.org/supplemental/10.1103/PhysRevLett.125.058002 further details on the CFV rate model and LCL EOS analysis for PVAC and P4ClS, the density scaling model and Tait EOS analysis for PVAC, the CFV model for films, and additional discussion on density near interfaces.
[36] D. Diaz-Vela, J.-H. Hung, and D. S. Simmons, ACS Macro Lett. **7**, 1295 (2018).
[37] K. Fukao, T. Terasawa, Y. Oda, K. Nakamura, and D. Tahara, Phys. Rev. E **84**, 041808 (2011).
[38] W. Heinrich and B. Stoll, Colloid Polym. Sci. **263**, 873 (1985).
[39] C. Roland and R. Casalini, Macromolecules **36**, 1361 (2003).
[40] R. Casalini, U. Mohanty, and C. M. Roland, J. Chem. Phys. **125**, 014505 (2006).
[41] R. Casalini and C. M. Roland, J. Non-Cryst. Solids **353**, 3936 (2007).
[42] I. Avramov, J. Non-Cryst. Solids **262**, 258 (2000).
[43] R. Casalini and C. M. Roland, Phys. Rev. Lett. **113**, 085701 (2014).
[44] A. Grzybowski and M. Paluch, in *The Scaling of Relaxation Processes*, edited by F. Kremer and A. Loidl (Springer International Publishing, Cham, 2018), pp. 77–119.
[45] R. P. White and J. E. G. Lipson, Eur. Phys. J. E **42**, 100 (2019).
[46] R. P. White and J. E. G. Lipson, J. Chem. Phys. **147**, 184503 (2017).
[47] R. P. White and J. E. G. Lipson, Macromolecules **49**, 3987 (2016).
[48] P. Zoller and D. Walsh, *Standard Pressure-Volume-Temperature Data for Polymers* (Technomic Pub Co., Lancaster, PA, 1995).
[49] Y. Yi and P. Zoller, J. Polym. Sci. Part B-Polym. Phys. **31**, 779 (1993).
[50] G. Adam and J. H. Gibbs, J. Chem. Phys. **43**, 139 (1965).